# Energy-Transfer Editing in Lanthanide-Activated Upconversion Nanocrystals: A Toolbox for Emerging Applications

Xian Qin,[†] Jiahui Xu,[†] Yiming Wu,[†] and Xiaogang Liu*,[†,‡]

[†]Department of Chemistry, National University of Singapore, 3 Science Drive 3, Singapore 117543, Singapore
[‡]Center for Functional Materials, NUS Suzhou Research Institute, Suzhou, Jiangsu 215123, P. R. China

ABSTRACT: Advanced nanoscale synthetic techniques provide a versatile platform for programmable control over the size, morphology, and composition of nanocrystals doped with lanthanide ions. Characteristic upconversion luminescence features originating from the 4f−4f optical transitions of lanthanides can be achieved through predesigned energy transfer pathways, enabling wide applications ranging from ultrasensitive biological detection to advanced spectroscopic instrumentation with high spatiotemporal resolution. Here, we review recent scientific and technological discoveries that have prompted the realization of these peculiar functions of lanthanide-doped upconversion nanocrystals and discuss the mechanistic studies of energy transfer involved in upconversion processes. These advanced schemes include cross relaxation-mediated depletion, multipulse sequential pumping, and nanostructural configuration design. Our emphasis is placed on disruptive technologies such as super-resolution microscopy, optogenetics, nanolasing, and optical anticounterfeiting, which take full advantage of the upconversion nano-phenomena in relation to lanthanide-doped nanocrystals.
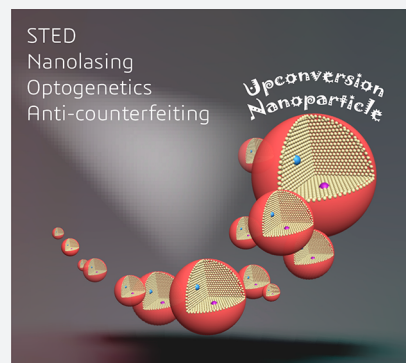
1. INTRODUCTION

Photon upconversion, an unusual nonlinear optical process, has attracted tremendous research interest due largely to its ability to realize frequency conversion without stringent constraints, such as the prerequisite of phase matching in second harmonic generation. Because of their abundant ladder-like 4f energy levels, lanthanide ions, when embedded in inorganic hosts, have proven effective in achieving photon upconversion through the successive absorption of low excitation energies followed by the emission of high-energy photons. The phenomenon of photon upconversion through lanthanides was first observed by Nicolaas Bloembergen in 1959 when he intended to count the number of infrared photons by colliding them with solid crystals doped with lanthanide or transition metal ions.[1] As an effective pumping source, the advent of lasers has significantly facilitated the development of upconversion luminescence materials, made evident in the pioneering works of François Auzel and of Ovsyankin and Feofilov.[2,3] To date, lanthanide-doped upconversion materials have been exploited for various applications by taking advantage of their ability to convert near-infrared (NIR) incident light into high-energy ultraviolet or visible emissions.[2,4,5]

The advent of nanotechnology provides a powerful tool to control the size of lanthanide-doped materials down to the nanometer length scale, with the smallest being ∼2 nm in diameter.[6] Unlike quantum dots dominated by size-dependent quantum phenomenon, the luminescence profiles of lanthanide-doped nanocrystals are hardly affected by miniaturization because of the direct pumping of the lanthanide ions and the

inertness of the lanthanide's 4f orbitals to its surroundings. Energy transfer within such a luminescence system occurs mainly among the dopants, which enables the modulation of the energy transfer pathways through spatial control over the dopant−dopant distance during the nanocrystal growth stage. For example, by deliberately controlling the doping concentration or the geometric structure, emission colors covering the entire visible spectral region can be achieved in lanthanide-doped upconversion nanocrystals since the intensity ratio between the different emission bands is critically dependent on the dopant−dopant distance.[7] Alternatively, full-color emission at single-particle levels can be obtained from multilayer core−shell structured nanocrystals that are sensitive to the laser pulse duration.[8] In addition, upconversion luminescence from lanthanide activators without long-lived intermediate states is accessible through the use of gadolinium-based core−shell nanoparticles.[9] These unique optical properties provide upconversion nanocrystals with unparalleled capabilities for applications that would otherwise be unattainable through their bulk counterparts (Figure 1).

Despite the considerable achievements over the past eight years, the low quantum conversion efficiency remains the key bottleneck that prevents the utility of upconversion nanocrystals for practical applications. Compared with bulk materials, the upconversion luminescence from nanocrystals suffers from more severe quenching due to a higher density of surface-bound activators, by which the excitation energy is dissipated
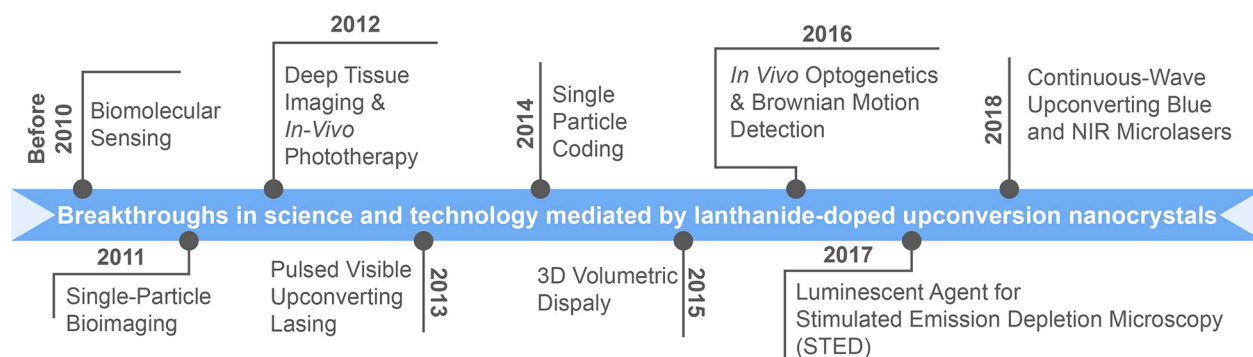
Figure 1. Representative scientific and technological breakthroughs through the development of functionalized upconversion nanocrystals.

nonradiatively. Hence, the structural configuration and composition of the nanocrystals need to be precisely controlled during the synthesis, which poses added constraints in the manipulation of luminescence profiles. On a separate note, these constraints are likely to stimulate researchers to develop innovative and effective solutions. Indeed, impressive progress has been made over the past few years in upconversion luminescence enhancement through modification of the energy transfer processes such as surface passivation, pumping scheme design, host matrix selection, surface plasmonic coupling, and photonic crystal modulation.[10,11]

In view of the already extensive literature on upconversion nanocrystals, we focus here on recent developments in which energy transfer-governed upconversion emission could be realized through intrinsic structural and compositional control as well as different modes of external stimulation. We begin with a brief description of the basic principles underlying the upconversion process, followed by discussion of the major challenges in improving the optical performance of upconversion nanocrystals. We also review the recent use of upconversion nanocrystals to provide multilevel anticounterfeiting, perform super-resolution microscopy, interrogate neural circuitry, and investigate upconversion lasing. The emphasis is placed on emerging areas in which upconversion nanocrystals show particular advantages over their widely used optical material counterpart, organic dyes.

2. FUNDAMENTALS

2.1. Upconversion Mechanism. A given upconversion nanocrystal usually consists of an inorganic host matrix and lanthanide dopants that typically occupy the lattice sites. When lanthanide ions sense the crystal field of the host lattice, the probability of optical transitions within the 4f manifolds can be greatly enhanced due to the relaxation of the spectroscopic selection rule. Unlike traditional semiconductors, upconversion nanocrystals principally do not feature host-sensitized emission. Instead, the lanthanide dopants serve as active luminescence centers that are responsible for excitation energy absorption, energy transfer, and radiative emission processes. Upconversion mechanisms can be generally categorized into excited state absorption (ESA), energy transfer upconversion (ETU), photon avalanche (PA), cooperative energy transfer (CET), and energy migration-mediated upconversion (EMU). Among these five mechanisms, ETU has been demonstrated to be the most efficient process. In the simplest ETU system, two types of lanthanides, namely, sensitizers and activators, are codoped to enable high efficiency energy harvesting and emission. Although the energy transfer process prevails in the

ETU mechanism, this process has also been widely observed in nanocrystals governed by PA, CET, and EMU mechanisms. In addition, the ESA process may occur concurrently with other processes when a given upconversion system encounters an appropriate level of pumping energy. By comparison, the EMU process mainly occurs in a core−shell particle comprising energy migrators, which can effectively bridge the excitation energy from the sensitizer to the emitter across multilayered interfaces. This design enables the minimization of deleterious cross relaxation between distinct lanthanide ions, thus resulting in drastic upconversion amplification from a series of activators without ladder-like intermediate states.[9] As the mechanistic investigation is beyond the scope of this review, readers are encouraged to refer to previously published reviews and tutorials for more details.[12−15]

2.2. Energy Transfer Efficiency. Achieving a high upconversion efficiency is of paramount importance to practical applications. Despite significant efforts, the conversion efficiency of nanocrystals remains much lower than that of their bulk equivalents, as evidenced by the reported low quantum yield ($\sim 0.1\%$) of $NaYF_4$:Yb,Er nanoparticles with a diameter of 30 nm.[16] Apart from the intrinsic parity-forbidden nature of 4f−4f optical transitions, the typically low conversion efficiency arises mainly from the presence of surface quenchers such as lattice defects and solvent molecules, which suppress the effective energy transfer through nonradiative decay. Owing to the high surface-to-volume ratio of nanocrystals, a major task of nanocrystal design lies in understanding how surface quenchers disturb the energy transfer process.

> Owing to the high surface-to-volume ratio of nanocrystals, a major task of nanocrystal design lies in understanding how surface quenchers disturb the energy transfer process.

The energy transfer pathways in a given nanocrystal could be divided into four classes: (i) ion−ion energy transfer, (ii) ion-defect energy transfer, (iii) ion-ligand energy transfer, and (iv) particle−particle energy transfer, as illustrated in Figure 2. Notably, for class (i), energy transfer is possible not only between lanthanide ions but also between lanthanide and transition metal ions. Given the distance dependence of the energy transfer rate, the determination of the dopant distribution in a nanoparticle of interest is critical. In general,
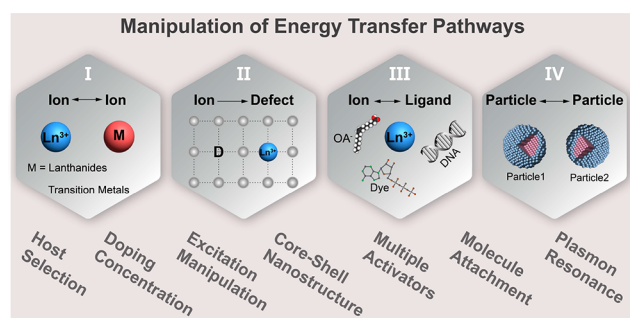
Figure 2. Schematic illustration showing four major energy transfer pathways dominated in upconverting nanosystems. A list of chemical and physical approaches to energy transfer manipulation is included in the scheme.

the core of the nanoparticle inherits the atomic arrangement from its bulk counterpart, where the crystallinity is essentially maintained. Instead of occupying interstitial sites, lanthanide ions or other types of metal dopants tend to statistically substitute for host cations featuring a similar valence charge, as recently confirmed by high-resolution scanning transmission electron microscopy.[17] There is a general consensus that the distance between dopants can be estimated using the crystallographic parameters of the host lattice. However, this theorem does not hold for small nanoparticles with high surface areas. For example, when doped into a $NaGdF_4$ nanocrystal, Tb^{3+} and Nd^{3+} were found to preferentially replace Gd^{3+} in center and edge sites, respectively, irrespective of the similar ionic radius among these lanthanide ions.[18] In another study, trivalent Pr, Tb, and Dy ions were observed to occupy sites mainly on the surface of SnO_2 nanoparticles, while Eu^{3+} and Sm^{3+} showed multimodal distributions.[19] Clearly, such nonstatistical distribution of dopants in nanocrystals may complicate the determination of the dopant−dopant distance and thus impede the estimation of the energy transfer rate.

Importantly, the number of lattice defects can increase rapidly in nanoparticles, with most residing on the surface of the nanoparticles. Moreover, heterovalent doping usually requires the formation of particular defects to maintain the entire system in the neutral state. Accordingly, the existence of defects not only complicates the process of distance measurement but also leads to unwanted nonradiative energy transfer between dopants and defects,[20] as seen in the case of type (ii) energy transfer. Unfortunately, the excitation energies stored in the defect sites usually dissipate through the vibration of the host lattice in the form of heat. The currently reported models for the calculation of the energy transfer rate do not account for the probability of ion-defect pathway-mediated energy transfer, which may lead to unavoidable deviation from the actual process of energy transfer within nanoparticles.

The type (iii) energy transfer pathway is associated with the interaction between the dopant ions and the ligands attached to the surface of a given nanoparticle. This interaction arises because ligands are often required for stabilizing the nanoparticles in solvents. Such pathways can be seen in two different scenarios. One is that the surface dopants directly chelate with the ligands, resembling the formation of lanthanide-based complexes.[21] In the second case, energy transfer can occur between the ligands and the dopants resting at the subsurface or even in the center of the particles, depending on the actual dopant−ligand distance.[22−24] When

constructing a model for the calculation of this transfer rate, these two scenarios should be equally considered.

As the particle size continues to decrease, the energy transfer (type iv) via particle−particle channels becomes important, especially for nanofluids with high particle concentrations. The distance between these nanoparticles can be dictated by adopting specific ligands with extended carbon chains of different lengths.[25] Interestingly, particle−particle energy transfer could endow the nanosystem with intriguing upconversion emission profiles accessible by self-assembled nanostructures.[26−28] Thus, the contribution of the particle−particle channel to the transfer rate should be carefully examined.

2.3. Energy Transfer Manipulation. Energy transfer is an essential process in upconversion, and its manipulation has been demonstrated to be effective for tuning emission profiles, such as emission color and lifetime. On the other hand, energy transfer from dopants to surface defects or ligands could lead to a substantial decrease in upconversion efficiency. In this subsection, we summarize common strategies that are currently implemented to regulate the energy transfer process.

In light of the competition between the different energy transfer processes, the precise determination of the transfer rate for a specific pathway has been challenging. In general, the key factors affecting energy transfer include ion distribution, wave function coupling, and energy overlap integral. Varying the distribution of the dopants is the most straightforward approach to tuning the type (i) energy transfer process. For instance, an increase in the doping concentration facilitates cross relaxation between dopants as a result of the reduced ion−ion distance. Another method to control the ion distribution is to identify particular hosts in which lanthanide ions tend to segregate in the form of chains or clusters upon host cation substitution.[29] As such, intriguing luminescence phenomena, such as five-photon upconversion[30] and single-band emission,[31] can be achieved. The intercalation of additional metal ions (Cd^{2+}, Mn^{2+}, Fe^{3+}, etc.) may also alter the ion distribution in the host lattice.[32,33]

Nanoparticle synthesis is a trivial process in which the formation of surface quenchers occurs spontaneously and subsequently amounts to added channels for unwanted energy transfer (type ii and iii).[34,35] For example, the unexpected incorporation of hydroxyl ions (OH^-) into nanoparticles could reduce upconversion conversion efficiency.[35] Currently, the most effective approach for eliminating surface quenchers is to grow an optically inert shell onto the bare core nanoparticles. The effectiveness of such core−shell structures for the suppression of nonradiative emission has been validated, as evidenced by the enhanced upconversion luminescence upon the removal of surface quenchers through core−shell engineering.[17,36] The core−shell design could be used to suppress the deleterious process of cross relaxation by enlarging the dopant−dopant distance, thus maximizing the upconversion efficiency.[37] Apart from surface passivation, a core−shell design can also be used to design the energy transfer pathways and allow the realization of novel upconversion features, including full-color emission[8] and new activator development.[9] For more details, readers are encouraged to refer to the work of Chen et al., in which the criteria and recipes for core−shell nanoparticle design and synthesis are well summarized.[38]

In addition to the manipulation of the particle's composition and structure, the amplification in local electromagnetic field by coupling noble metals has also proven effective in drastically
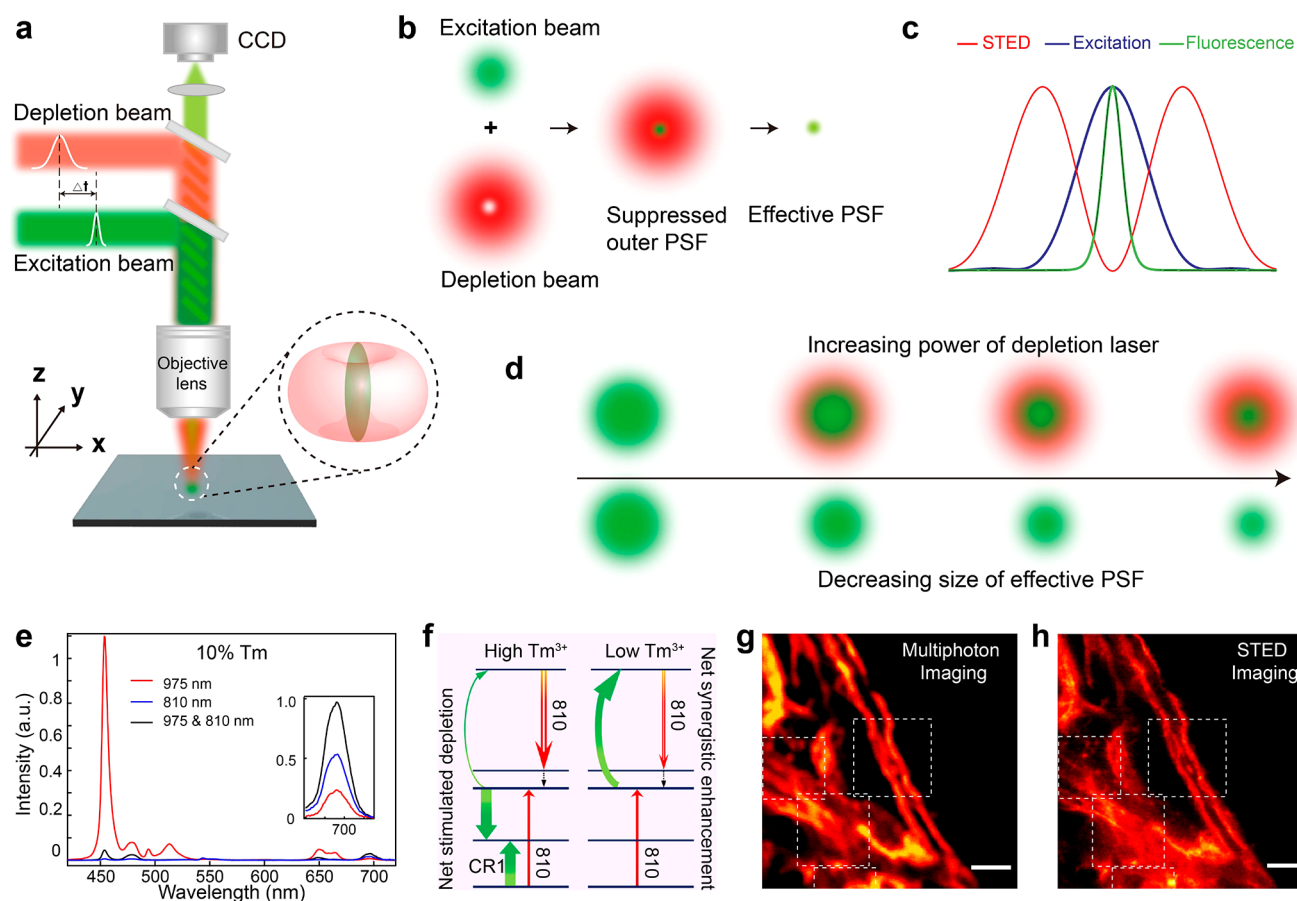
Figure 3. (a) Schematic diagram of a simplified STED experimental setup. (b, c) A scheme showing the effective point spread function (PSF) achieved by overlaying the excitation beam with the donut-shaped depletion beam. (d) A scheme showing the decrease in the size of the effective PSF obtained by increasing the intensity of the depletion laser. (e) Emission spectra of NaYF$_4$:18%Yb/10%Tm nanoparticles upon different wavelength excitations. Note that 96% depletion efficiency of the 455 nm emission can be achieved by simultaneously implementing 980 nm CW excitation and 810 nm CW depletion. (f) Schematic sketch of net cross relaxation-mediated stimulated depletion (left) and net synergistic enhancement (right), typically observed from upconversion nanocrystals with high and low Tm^{3+} doping concentrations. (g, h) High resolution imaging, in multiphoton mode and STED mode, of cytoskeleton structures and desmin proteins in HeLa cancer cells. Panel d reproduced with permission from ref 58. Copyright 2013 Frontiers. Panels e−f reproduced with permission from ref 67. Copyright 2017 Nature.

enhancing upconversion efficiency.[10,39−41] Such plasmon-mediated upconversion enhancement is generally ascribed to the increase in the incident pumping flux or radiative decay rate.[42−45] Of particular note is that the effect of surface plasmons on the energy transfer has been decoupled from the aforementioned enhancement in upconversion absorption and emission processes.[46−49] The manipulation of energy transfer through plasmonic resonance can significantly benefit practical applications, such as upconversion-mediated photovoltaics and bioimaging, in which low-power irradiance is highly desirable. Given the distance-dependent plasmon-enhanced upconversion, the structure and shape of plasmonic materials in the form of sphere, rod, pillar/hole array, and core−shell particle need to be exquisitely designed to maximize the upconversion enhancement.[43,45,50]

3. EMERGING APPLICATIONS

Over the past few years, the rapid development of nanoparticles with multimodal functionalities has allowed the applications of nanoparticles to be expanded from biomolecular sensing[51,52] to deep-tissue imaging,[53] lighting,[54] and the measurement of the instantaneous Brownian velocity.[55] In this section, we attempt to highlight the broad utility of

upconversion nanoparticles in super-resolution microscopy, optogenetics, lasing, and multilevel anticounterfeiting.

3.1. Super-Resolution Microscopy. Luminescent biomarkers, when combined with microscopic imaging techniques, have been demonstrated to be effective for visualizing tissue structures and the dynamics of physiological processes. However, the application of such imaging techniques in the life science is often hampered by low spatial resolution. By employing an organic dye-based luminescent probe, the best lateral resolution that a given far-field optical microscope can achieve is approximately half the wavelength of the excitation light. Such distance resolution between two point objects was defined as the diffraction limit by Abbe in 1873.[56] Thus, the optical resolution is usually ∼200 nm laterally and ∼500 nm axially, which is far too large for the precise tracing of biological events, which typically occur at scales of a few to tens of nanometers.

Given the luminescence nature of the markers, subdiffraction resolution can be achieved by partially switching on or off the emission originating from a specific area of the phosphors under study. To date, many far-field fluorescence microscopies have been developed for super-resolution imaging such as stimulated single-molecule localization nanoscopy, saturated

structured illumination microscopy, and stimulated emission depletion microscopy (STED). In this section, we review the development of upconversion nanoparticle-associated STED nanoscopy and its utility for bioimaging.

The STED technique typically involves the use of a dual-laser system: one laser beam as the excitation source and the other one with a donut-shaped focal spot for emission depletion. Upon the excitation of a fluorophore, the second beam source is able to switch off the luminescence of the fluorophore at the donut-shaped periphery (Figure 3a). The size of the emission spot is thereby significantly reduced, and the lateral resolution is subsequently improved, as illustrated in Figure 3b−d. To date, many STED microscopes with different modalities have been developed for high-resolution bioimaging.[57,58] Despite considerable efforts, further advancement in the performance of STED microscopy has been hindered by the inherent limitations associated with conventional optical contrast agents, including photobleaching, photoblinking, autofluorescence, and a shallow imaging depth. In addition, the operation of these optical materials usually requires high-power depletion lasers, which may induce light toxicity and aggravate the degree of photobleaching.

In contrast to conventional biomarkers, lanthanide-doped upconversion nanoparticles allow deep-tissue labeling and imaging to be performed without photobleaching and photoblinking. Moreover, the overheating-induced toxicity can be effectively circumvented by choosing an appropriate lanthanide sensitizer that has absorption in biological windows.[59−63] With the help of the STED technique, researchers have demonstrated subdiffraction imaging using upconversion nanoparticles. The first demonstration of such efforts was reported in 2011 by Kolesov et al., who showed that an optical resolution of 50 nm could be achieved upon the excitation of Pr-doped YAG ($Y_3Al_5O_{12}$) ultraviolet-emitting nanoprobes.[64] Notably, instead of emission depletion, stimulated excited state absorption is responsible for breaking the diffraction limit. However, their method is not suitable for bioimaging because the excitation and emission wavelengths under study fall short of the biological window. In another study involving $NaYF_4$:Yb/Er nanoparticles, stimulated excited state absorption was again recognized as the main cause of the enhancement of the imaging resolution, when illuminated by two NIR beams simultaneously.[65] Despite the high brightness and deep-tissue penetration ability enabled by these fluoride-based nanoparticles, the reported maximum depletion efficiency of the green emission is merely 30%, leading to a relatively low signal-to-noise ratio.

> In contrast to conventional biomarkers, lanthanide-doped upconversion nanoparticles allow deep-tissue labeling and imaging to be performed without photobleaching and photoblinking.

In 2017, a classical stimulated emission depletion was observed by Jin and co-workers in highly doped $NaYF_4$:Yb/Tm nanoparticles upon concurrent illumination with 980 and 808 nm lasers.[66] The researchers argued that the cross relaxation-induced population inversion between the intermediate state and the ground state is a prerequisite for the

successful depletion of the blue emission originating from Tm^{3+} emitters. Notably, the switch-off efficiency of the blue emission can reach 90% to result in a substantial reduction in the lateral resolution down to 28 nm. The cross relaxation in highly doped nanoparticles not only enables stimulated emission but also significantly lowers the threshold of the depletion intensity compared to the one used for conventional probe depletion.

A similar depletion phenomenon was reported by Zhan and He and their co-workers (Figure 3e).[67] However, the researchers claimed that stimulated depletion occurs between higher-lying excited states and intermediate states rather than the optical transition between intermediate and ground states, as depicted in Figure 3f. Additionally, cross relaxation was found to compensate for stimulation-induced upconversion enhancement, accompanied by a reduction in the depletion intensity. Apparently, the way by which the cross relaxation-associated energy transfer prompts the depletion of the emission requires further mechanistic study.

> Further improvement in the upconversion-based imaging resolution requires a considerable reduction in the particle size. However, the synthesis of small nanoparticles with a high upconversion efficiency remains a challenge because they often suffer from severe surface quenching.

By view of the existence of abundant energy levels in lanthanides, their optical population can be depleted by different stimulation sources at specific wavelengths. For example, apart from the 800 nm-induced depletion of the blue emission of $NaYF_4$:Yb/Tm nanoparticles, both the blue and red emissions of these nanoparticles can also be quenched by combining 980 and 1550 nm lasers.[68] Such a mode of operation can also be employed to suppress the red emission of $NaYF_4$:Yb/Er nanoprticles.[69] More interestingly, two-color super-resolution imaging has also been demonstrated by using a mixture of $NaYF_4$:Yb/Tm and $NaGdF_4$:Yb/Tm@$NaGdF_4$:Tb nanoparticles as luminescent markers, by which only one pair of excitation-depletion beams is needed.[67]

Lanthanide-doped upconversion nanoparticles have been considered as promising probes for imaging cellular structures both in vitro and in vivo. When coupled with the STED technique, these nanoparticles allow the visualization of subcellular fine-structures with high spatial resolution. The proof-of-concept study was first validated in the case of the cytoskeleton imaging of HeLa cells using 12 nm $NaGdF_4$:Yb/Tm nanoparticles (Figure 3g,h).[67] The dual-beam operation at 975 and 810 nm enabled subcellular imaging with a lateral resolution of 82 nm.

Further improvement in the upconversion-based imaging resolution requires a considerable reduction in the particle size. However, the synthesis of small nanoparticles with a high upconversion efficiency remains a challenge because they often suffer from severe surface quenching. To boost the imaging contrast, the most straightforward approach is to increase the
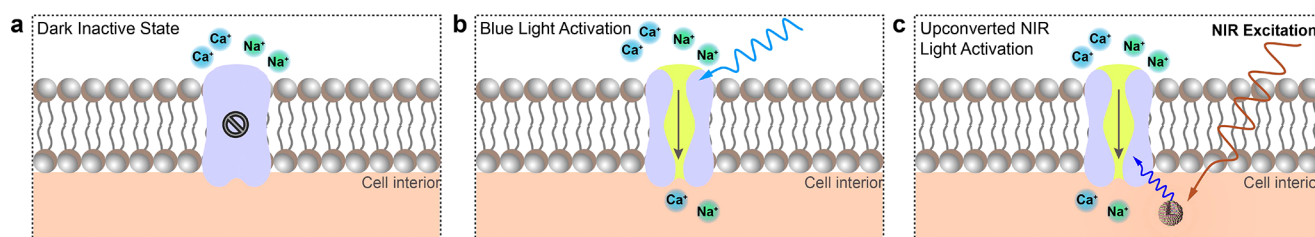
Figure 4. Schematic illustration of the underlying mechanisms of optogenetic control through ChR2 protein over the opening/closing of ion channels in a cellular membrane. Ca^{2+} and Na^+ can access the interior cell when ChR2 is activated upon 470 nm irradiation, resulting in membrane depolarization and neuronal signal firing. (a) The ion channel protein ChR2 is initially blocked in the dark. (b) ChR2 opens for cation transportation when excited by blue light. (c) Activation of the ChR2 channel through the use of upconversion nanoparticles upon 980 nm excitation.
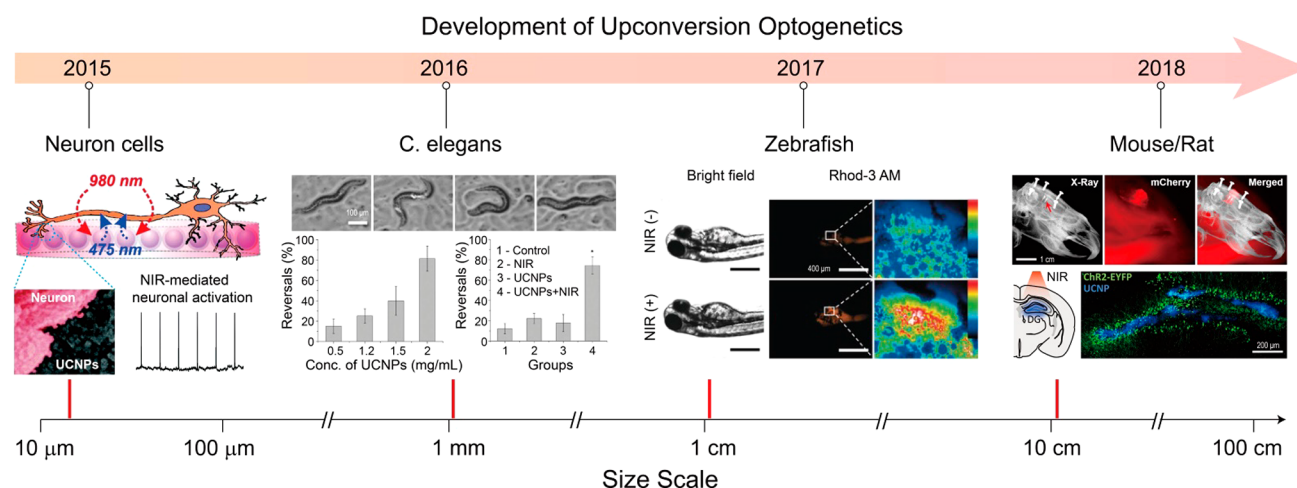

Figure 5. Representative upconversion nanoparticle-associated optogenetics in vitro and in vivo. From left to right, cell, worm, fish, and mouse. Neuron cells. Top: Schematic illustration showing the use of polymer−nanocrystal hybrid scaffolds for neuron activation. Bottom: The magnified neuron−nanocrystal interface (left) and the repetitive potentials of a current−clamped hippocampal neuron evoked by 980 nm light irradiation (right). *Caenorhabditis elegans*. Top: Representative images showing the upconversion-mediated optogenetic reversal behavior of a worm with ChR2 expression in their mechanosensory neurons. Bottom: The correlation of the reversal response percentage with the concentration of the incubated upconversion nanocrystals (bottom left) and the recorded reversal response percentage under four types of experimental conditions. Zebrafish. In vivo photoluminescence imaging of zebrafish incubated with upconversion nanoparticles. Scale bar is 10 μm. Mouse. In vivo upconversion optogenetics. Top: X-ray and fluorescence images of the implanted micro-optrodes and the regions expressing ChR2 opsin. Bottom left: Schematic illustration showing transcranial NIR stimulation of the hippocampal engram for memory recall. Bottom right: Optical images of upconversion nanocrystals (blue) and EYFP-labeled ChR2 protein (green) in the dentate gyrus of a mouse. Panel Neuron cells reproduced with permission from ref 71. Copyright 2015 Royal Society of Chemistry. Panel *C. elegans* and panel Zebrafish reproduced with permission from refs 74 and 75. Copyright 2016 and 2017 Wiley. Panel Mouse/Rat reproduced with permission from refs 78 and 80. Copyright 2017 Elsevier Science and 2018 Science.

amount of nanoparticles, which may induce undesired physiological toxicity to biological species. Upconversion nanoparticles may not be suitable for fast scanning imaging as a streaking effect, due to the long decay time of the lanthanide emission, is often encountered. To overcome this drawback, a decrease in the pixel dwell time is likely to counteract this negative effect. Additionally, the improvement of the axial resolution and the simplification of the technological complexity need to be well addressed before STED nanoscopy can be widely deployed for clinical bioimaging.[57]

3.2. Optogenetics. Optogenetics has been touted as a revolutionary biotechnology that allows neuromodulation via the optical stimulation of photoresponsive proteins. Upon illumination at a specific visible wavelength, proteins such as Channelrhodopsin-2 (ChR2) and C1V1 (a red-shifted opsin with several variants) will be activated to open light-gated ion channels and subsequently induce membrane depolarization (Figure 4a,b). The light stimulation can also close the ion

channels, depending on the type of opsin proteins under investigation. Despite their enticing prospects, the advancements of optogenetic techniques for in vivo applications are hampered, mainly due to poor tissue penetration of visible light. To alleviate the light attenuation, traditional optogenetic approaches usually require the implantation of optical fibers for light transport during in vivo experiments. Obviously, the implantation of fiber optics damages the tissue along its path, disturbs the physiology of organs, alters neuronal function, and imposes movement constraint and behavioral limitation in wake subjects.

Upconversion nanoparticles can serve as remote light transducers for the minimally invasive control of deep-tissue neuronal activities (Figure 4c). The concept of using upconversion nanoparticles for optogenetics was first proposed in 2011 by Deisseroth and Anikeeva.[70] It was not until 2015 that optogenetic-based brain stimulation became more prominent in the field of neuromodulation. Several groups independently studied the feasibility of using upconversion

nanoparticles to activate opsin proteins via remote NIR light irradiation both in vitro and in vivo (Figure 5).[71−73] The size of the biosamples ranged from 10 μm cells to 10 cm rodents. Studies of neurons, cultured or simply mixed with upconversion nanoparticles, revealed that an inward current response can be detected upon remote 980 nm light illumination.

Compared to in vitro experimentation, the realization of deep-tissue penetration is of paramount importance for in vivo research. In 2015, without the need for implanted optical fibers, the groups of Han and Zhou successfully demonstrated that the incorporation of $NaYF_4$:Yb/Tm@$NaYF_4$ nano-transducers allows the remote control of deep-tissue signaling events in response to Ca^{2+}-dependent immune systems in mouse models.[73] In early 2016, the successful activation of ChR2 using $NaYF_4$:Yb/Tm nanoparticles in *Caenorhabditis elegans* was reported, as evidenced by the reversal response of the worms (Figure 5).[74] In another in vivo experiment on zebrafish larvae, $NaYF_4$:Yb/Tm/Nd@$NaYF_4$:Nd core−shell nanoparticles were specifically conjugated onto ChR2-express-ing cell surface by means of metabolic glycan biosynthesis (Figure 5).[75] In another study, precise subcellular stimulation was demonstrated through the specific attachment of $NaYbF_4$:Tm@$NaYF_4$ nanoparticles onto live HeLa cells.[76] It is of great value to mention that lanthanide-doped nano-particles can also be used for multiplexed neuronal inter-rogation, by which the simultaneous activation and inhibition of different opsin proteins can be achieved.[77]

In two separate reports, upconversion nanoactuator-mediated optogenetics were validated for deep-brain stim-ulation in mammals (Figure 5).[77−80] Specifically, Shi and co-workers developed a small implantable microdevice comprising $NaYF_4$:Yb/Er@$NaYF_4$ nanoparticles. This microdevice pro-vides a tetherless method to remotely trigger spiking activities in rat brains even at a tissue depth of 1 cm.[77−79] In a rather different approach, the Liu and McHugh groups demonstrated the in vivo NIR optogenetic control of multiple neuronal systems in a minimally invasive manner by the local injection of $NaYF_4$:Yb/Er-based nanoparticles.[80] Compared to systemic delivery through the blood, such a direct injection can bypass the diffusion barrier between the blood vessels and brain tissue, ensuring the delivery of the required concentration within selective space for effective optical stimulation. In addition to the control of neural activities, upconversion nanoparticle-based optogenetic tools can also be used as a therapeutic method for controlling the apoptotic signaling pathway of cancer cells, as demonstrated by the work of Zheng et al.[81]

Despite those developments described above, the use of upconversion nanoparticles for clinical optogenetics remains a formidable challenge. One of the main reasons lies in the inadequate amount of light harvesting because of the low efficiency of the photon upconversion process. To improve the light harvesting for neuronal activation, a high concentration of upconversion nanoparticles is generally needed. However, the random diffusion of the nanoparticles taking place in biological media or tissues may lead to a high level of physiological toxicity. Although the encapsulation of nanoparticles in the form of an optotrode provides a feasible solution to random diffusion,[78] such increase in the size of the nanotrasducer could cause irreversible damage and inflammation in the host of tissues.

High-power laser pumping could also be considered as an alternative method to improve the upconversion effi-ciency.[82−84] However, a high pumping power at 980 nm can cause overheating in biological media and tissues because water molecules absorb at 980 nm. Alternatively, the effect of overheating can be significantly alleviated by using dye- or Nd^{3+}-sensitized nanoparticles that are excitable at 800 nm.[75,85] Additionally, high upconversion efficiency can also be achieved with the help of a quasi-CW laser.[74] The quasi-CW laser does not cause overheating, even at a peak power of 4 W.

For clinical applications, the effect of body fluids on the optical properties of nanoparticles and their long-term toxicity requires a systematic study. The plasticity of the brain could also be another key factor that determines the performance of such optogenetic tools since maintaining continuous changes in neuronal networks may require different patterns of stimulation. The optical properties of nanoparticles must be adjustable according to specific physiological conditions.[86] However, such changes can also lead to variation in the physical distance between the opsin proteins carrying ion channels and the nanoparticles. In summary, upconversion nanoparticle-mediated optogenetics remains in its infancy and truly deserves further fundamental and technical investigation to deepen our understanding of the complex chemical and physiological reactions occurring in the human brain.

3.3. Upconversion Lasing. Stimulated emission, in laser action, has found broad applications including remote sensing, data storage, medical therapeutics, and photochemistry. With the advance in crystal growth technology, numerous solid-state lasers as alternatives to traditional gas- and liquid-phase lasers have been successfully developed since the 1980s, with emission wavelengths covering the near-ultraviolet, visible, and NIR ranges. In particular, deep-ultraviolet lasing has the potential to revolutionize precision engineering due to its intrinsic characteristics such as a high photon energy and high beam quality. To achieve such lasing, approaches involving excimers, wide bandgap semiconductors, and nonlinear optical or upconversion materials have been proposed. Upconversion-mediated lasers are particularly attractive, enabling high-efficiency lasing in the near-/deep-ultraviolet spectral region. More importantly, the realization of upconversion has less stringent requirements such as phase matching, thus simplifying the pump dynamics.

The first demonstration of an upconversion laser can be traced back to 1971 in Yb^{3+}- and Ho^{3+}-codoped BaY_2F_8 bulk materials.[87] Such a laser emits light with a wavelength of 554 nm when operated at cryogenic temperatures. Since then, lanthanide-based upconversion lasers with a wide tuning range of wavelength have been developed and summarized by Richard Scheps based on different upconversion processes.[4] Despite these achievements, the development of deep-ultraviolet upconversion lasing in bulk materials remains challenging, largely due to the low pump efficiency of four- or five-photon upconversion. Room-temperature operation can further complicate the design of laser components. This deficiency arises because the increase in temperature would depopulate higher excited states and induce excited state absorption, thus restraining the population inversion for lasing.

Emerging nanotechnology has provided researchers with a powerful tool to precisely tune the transfer pathways of excitation energies within a given material through rational design at the nanoscale. In light of the distance-dependent energy transfer nature of lanthanides, the structural engineer-ing of nanocrystals allows significant enhancement in the stimulated upconversion emission. For example, the occur-
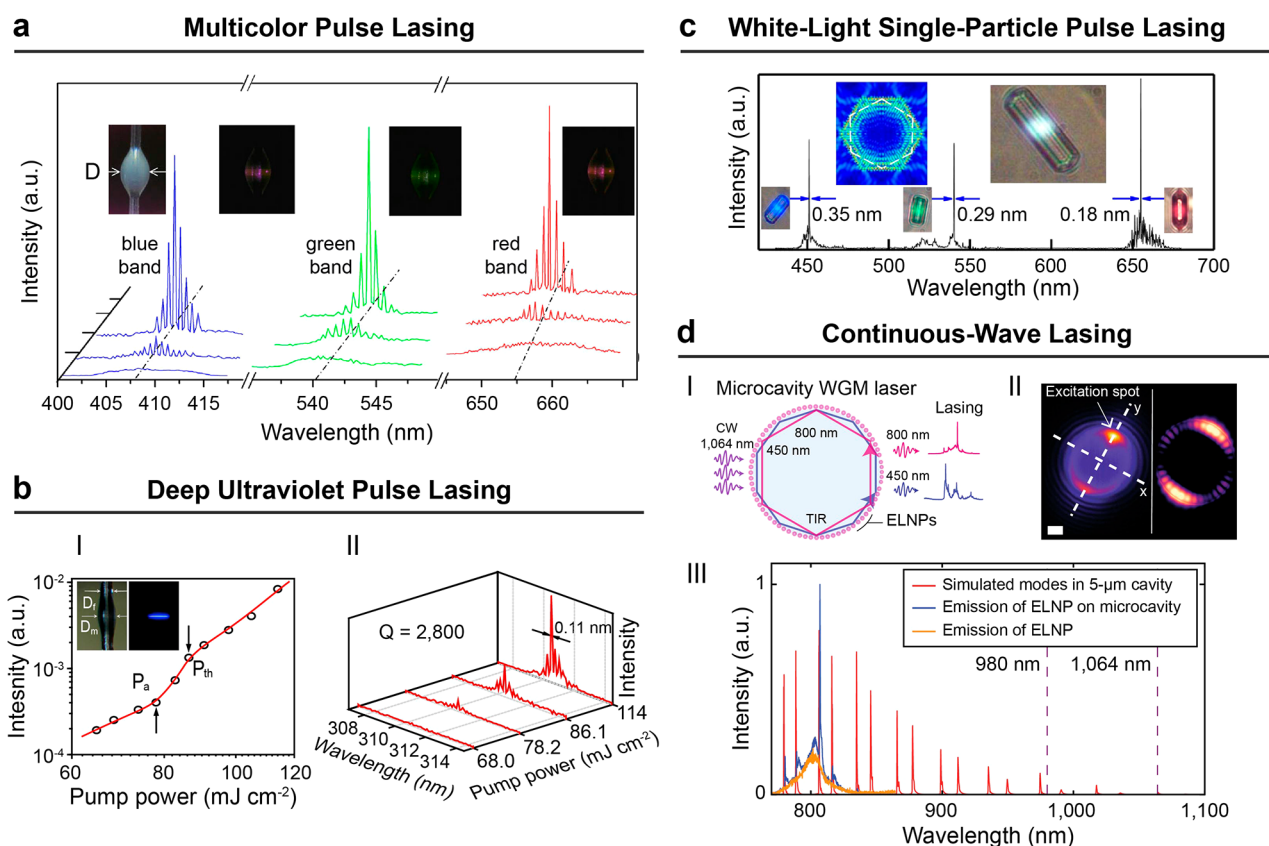
Figure 6. Upconversion nanocrystal-based lasing. (a) Multicolor pulse lasing spectra observed from a microcavity in a bottle-like geometry with a diameter (D) of 80 μm. The insets are images of the microcavity under different excitation powers. (b) Room-temperature deep-ultraviolet pulse lasing achieved through the use of a rationally designed microresonator. I: Plot of the intensity output versus the excitation power for a microresonator (D_m = 75 μm). The insets are the images of the microresonator with and without optical excitation. II: The lasing spectra of the microlaser at different excitation powers (D_m = 75 μm). (c) Room-temperature lasing spectra of three upconversion microrods (~3 μm in radius) upon 980 nm excitation. The three small insets are the corresponding optical images, while the two large insets are the simulated optical field distribution within a microrod that emits at 654 nm and the optical image of a microrod (~4 μm in radius) that emits white light lasing. (d) Continuous-wave lasing achieved by coupling energy-looping nanoparticles (ELNPs) to whispering-gallery modes of polystyrene microspheres. I: Schematic illustration showing the excitation and lasing occurring within the nanoparticle-coated microbeads. TIR stands for total internal reflection. II: Left: Wide-field image of the given lasing microbeads showing optical modes circulating within the resonator. Right: x−y plane projection of the simulated field distribution within a 5-μm polystyrene microsphere. Scale bar: 1 μm. III: Compiled emission spectra of the nanoparticles and the corresponding particle-coated beads, along with the simulated NIR spectra of whispering-gallery modes supported by a microsphere with a diameter of 5 μm. Panels a and c reproduced with permission from refs 88 and 90. Copyright 2013 and 2017 American Chemical Society. Panels b and d reproduced with permission from refs 89 and 91. Copyright 2016 and 2018 Nature.

rence and amplification of stimulated emission have been investigated in NaYF$_4$:Yb/Tm nanocrystals for super-resolution fluorescence microscopy.[66,67] Population inversion was detected in highly Tm^{3+}-doped nanocrystals upon NIR laser irradiation, making these nanomaterials particularly suitable as the gain media for upconversion lasing.

In 2013, Wang and Yu and their co-workers fabricated a room-temperature microlaser based on NaYF$_4$:Yb/Er@NaYF$_4$ nanocrystals as the gain medium (Figure 6a).[88] They developed a three-pulse excitation scheme and achieved sufficient population inversion without optical and thermal damage. Laser cavity configuration, either in a bottle-like geometry or in a classic Fabry−Perot cavity, is also crucial in generating lasing. To achieve deep-ultraviolet stimulated emission, the same groups further refined both the pumping scheme and the structure of the nanoparticles. By employing a similar bottle-like microresonator, the researchers observed deep-ultraviolet lasing at 311 nm upon five-pulse irradiation at 980 nm (Figure 6b).[89] Recently, white-light lasing was observed from NaYF$_4$:Yb/Er/Tm microrods, within which a

whispering-gallery mode could be accommodated (Figure 6c).[90]

Another breakthrough in the field of upconversion nano-particle-based lasing was recently reported by Fernandez-Bravo et al., who used NaYF$_4$:Gd/Tm@NaGdF$_4$ nanoparticles to achieve continuous-wave upconverted lasing at 450 and 800 nm upon 1064 nm pumping (Figure 6d).[91] By depositing the core−shell nanoparticles onto a polystyrene microresonator, lasing without marked heat generation is possible as the threshold for population inversion in Tm^{3+}-doped nano-particles is greatly reduced. Compared to the 980 nm excitation beam, 1064 nm light is nonabsorbable by tissues. Heat-induced tissue damage can be effectively circumvented. These newly developed nanolasers open up a new avenue toward applications in bioimaging, biosensing, and deep-tissue optogenetics.

3.4. Anticounterfeiting. The development of high-fidelity anticounterfeiting techniques is currently in great demand due to the rise of global counterfeiting and forgery in high-volume, high-profit merchandise, including banknotes, trademark tags,
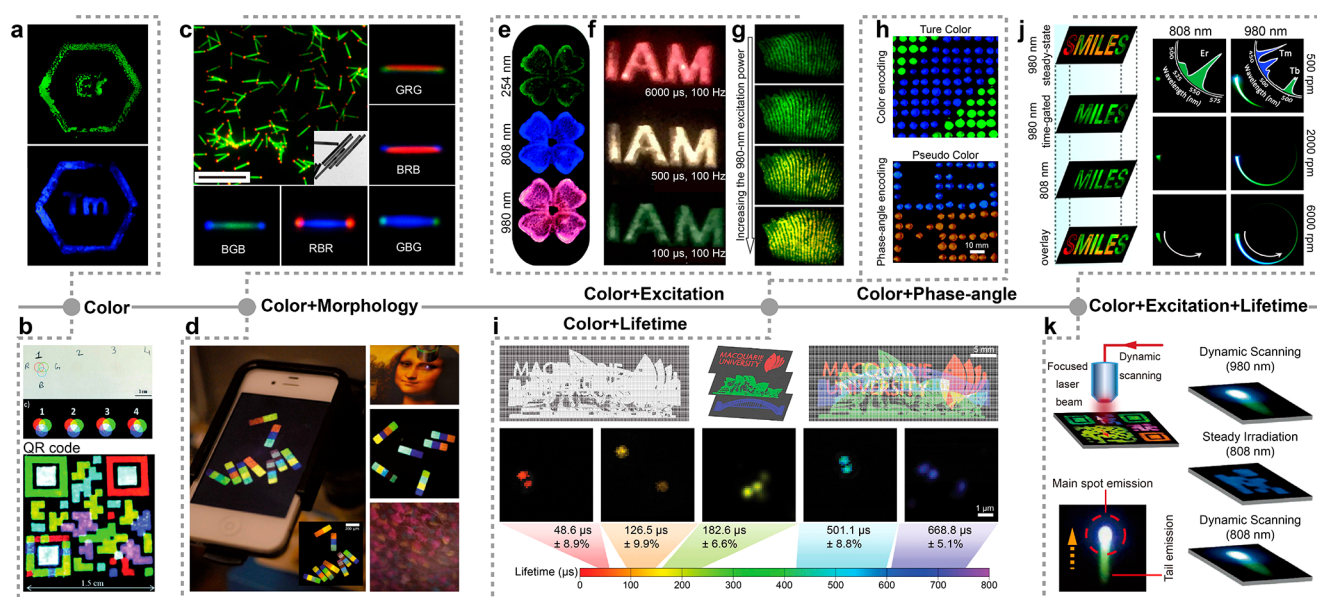
Figure 7. Representative upconversion nanocrystal-associated anticounterfeiting at different levels of security. (a) Optical decoding of encrypted papers through NIR light exposure. (b) Top: Red−green−blue printing using nanoparticle-based inks. Bottom: Optical image of the as-printed QR code featuring multicolor emission. (c) Multicolor barcoding in a single microcrystal. Scale bar: 2 μm. (d) Multicolor barcoding through upconversion nanoparticle-encapsulated polymeric microparticles. Scale bar: 200 μm. (e−g) Anticounterfeiting based on color and excitation characteristics. (h) Color and phase angle optical encoding. (i) Lifetime-encoded anticounterfeiting. Note that different colors represent different lifetimes. (j) Multilevel anticounterfeiting through the use of nanoparticles with different colors, lifetimes and pumping conditions. (k) Multilevel anticounterfeiting through Mn^{2+}-doped upconversion nanoparticles. Panels a, b, e, and h reproduced with permission from refs 92, 93, 99, and 104. Copyright 2014, 2016, and 2017 Royal Society of Chemistry. Panels c, g, and j reproduced with permission from refs 94, 103, and 106. Copyright 2014 and 2017 American Chemical Society. Panels d, f, i, and k reproduced with permission from refs 95, 102, 105, and 107. Copyright 2014 and 2017 Nature.

classified documents, and identity cards, as well as pharmaceutical products. Counterfeiting creates societal instabilities, triggers the infringement of intellectual property rights, and poses a great threat to medicine legislation.

Luminescence materials comprising lanthanide ions have been broadly considered as effective agents for the prevention of counterfeiting. For example, euro banknotes carry covert Eu(III)-containing pigments, which can emit a characteristic orange-red color upon UV excitation. By comparison, upconversion nanocrystals offers an added layer of security protection because they can be excited by both UV and NIR light. In this section, we will highlight recent advances in applying upconversion colloidal nanoparticles as security inks for anticounterfeiting.

Similar to conventional luminescent probes, the basic element for anticounterfeiting involving upconversion nanoparticles is the emission color, which is tunable from visible to NIR light.[7] Green-emitting NaYF$_4$:Yb/Er and blue-emitting NaYF$_4$:Yb/Tm nanoparticles are the most popular materials for upconversion-based anticounterfeiting measures (Figure 7a).[92] Nonetheless, a single-color emission hardly meets the criteria for multilevel and high-fidelity anticounterfeiting applications. One of the most straightforward strategies for enhancing the level of the security is to increase the range of emission colors. By mixing red-, green-, and blue-emissive upconversion nanoparticles in appropriate ratios, an arbitrary emission color can be achieved, depending on the percentages of the three primary colors. As a proof-of-concept, Meruga et al. printed invisible quick-response codes composed of colloidal upconversion nanoparticles. This invisible printing can be decrypted when illuminated with a 980 nm laser

(Figure 7b).[93] The design of multicolor and graphic encryption offers a dual level of security protection.

Although multicolored upconversion nanoparticles offer a large variety of colors, spectral overlapping may become a concern and can complicate the signal read-out. To overcome this problem, Zhang et al. developed an epitaxial end-on growth method to prepare microrods that could display different emission colors within a single microrod, as shown in Figure 7c.[94] This stripe-like emission feature was harnessed by the researchers to achieve security protection in documents. In a separate study, a universal microfluidics-based technique was adopted to pattern multicolor upconversion nanoparticles in the form of microscale barcodes.[95] As shown in Figure 7d, the emission brightness and color fidelity of these nanoparticles remained largely unaltered after the formation of the microscale barcodes. Another feasible approach to achieving multicolor emission is by mixing upconversion nanoparticles with their downshifting counterparts or other types of luminophores, such as quantum dots.[96−98] With the color output of the security inking materials being excitation-dependent, this approach offers another dimension of anticounterfeiting (Figure 7e).[99]

Anticounterfeiting based on a dual-modal manipulation of upconversion and downshifting luminescence can also be realized even on a single-particle level.[100,101] Using this approach, the purity and fidelity of the color can be largely preserved. By comparison, a simple mixing of nanophosphors displaying different colors under a single-wavelength excitation only produces superimposed color images. Upconversion emission, with high-purity and tunable chromatic colors, has been achieved through the use of multilayered core−shell nanocrystals, in which the color response is ultrasensitive to

the excitation wavelength and pulse frequency or duration.[8,102] As demonstrated by Huang and co-workers, the information on a printed document can be encrypted and decoded using pulse duration-sensitive $NaYF_4/Er@NaYF_4$ nanoparticles (Figure 7f). The pumping power-dependent modulation of emission color profiles could also be used as a convenient decoding method (Figure 7g).[103] By probing the kinetics of the upconversion luminescence, Zhang and co-workers demonstrated that phase angle control by tuning the luminescence rise and decay time could be used as another encoding modality for anticounterfeiting use (Figure 7h).[104]

In 2014, Jin and co-workers discovered that the lifetime of upconversion nanoparticles could be tuned from the microsecond to millisecond range (25.6 μs to 0.66 ms) by changing the dopant concentration.[105] The substantial change in lifetime was dictated by the concentration-induced variation in the ionic distance. Upon decoding with a time-gated microscope, lifetime-dependent patterns could be generated, as illustrated in Figure 7i. Recently, a platform combining color and lifetime modalities has been shown to be effective in enriching the capacities of upconversion nanoparticles for high-end encryption applications (Figure 7j).[106] In addition to lanthanides, transition metal ions such as Mn^{2+} featuring a long-lived emission decay, have been used for lifetime-based anticounterfeiting as well.[107] Considering that the emission lifetime of Mn^{2+} (39 ms) is 2 orders of magnitude longer than that of the lanthanides (0.6 ms), the emission is clearly distinguishable even by the naked eye without the need for any time-gated microscopy (Figure 7k).

It is important to note that the emission profile of the lanthanides could change in response to variation in temperature,[55,108] which makes the combination of upconversion nanoparticles and temperature control another viable approach for anticounterfeiting technology. Despite the enormous potential of upconversion nanoparticles for practical security applications, the process of decoding optically encrypted patterns could be a tedious task, particularly in regard to multilevel information decoding. Another practical limitation that also carries a major risk to upconversion-based anticounterfeiting is the requirement of strong coherent lasers with a high pumping power (>10 W/cm^2) for attaining visible emission.

4. CONCLUSIONS AND OUTLOOK

The combination of advanced nanotechnology and upconversion nanoparticles allows access to various emerging applications by harnessing the distinctive features of the upconversion luminescence. Although only four types of emerging applications are covered in this review, they provide the basis for new areas of research. For example, upconversion-mediated fluorescence emission difference microscopy[109] and NIR emission saturation nanoscopy[110] have also been developed as advanced super-resolution techniques for deep-tissue imaging. Notably, upconversion nanocrystal-associated applications are not absolutely isolated, and their combination would enable more functions and different capabilities that certainly cannot be achieved using any of these techniques alone. Combining STED microscopy with optogenetic tools may become extremely useful in the dynamic monitoring of neuronal activities in living cells or even in vivo with unprecedented precision.

The aforementioned applications take advantage of the upconversion nanophenomena enabled by editing nonradiative

energy transfer within nanostructured materials. In the meantime, radiative energy transfer, in which the emission of the sensitizer is reabsorbed by the activator, could also enrich the utility of upconversion nanomaterials toward energy harvesting such as upconversion-coupled photovoltaics.[111−113] By serving as a spectral converter, upconversion nanomaterials can largely minimize the nonabsorption of sub-bandgap photons when incorporated into solar cells in the form of particles or films. Most recently, upconversion-mediated perovskite photovoltaics has attracted intense research interests largely due to the large absorption coefficients and high photoluminescence quantum yields of the perovskite materials.[98,114,115] Given the noncoherent radiation nature of the sunlight, achieving efficient upconversion in these systems at low-power irradiance could pose a substantial challenge. To this end, the use of optical concentrators, plasmonic materials, or advanced photonic structures may provide a feasible solution.[41,116,117]

Despite the many proofs-of-concepts that have been demonstrated, the low conversion efficiency inherent to upconversion nanoparticles continues to prevent their practical utility. In that respect, it is essential to conduct a comprehensive mechanistic investigation of rudimentary upconversion processes, including excitation absorption, energy transfer, and excited state dynamics. Among them, energy transfer within the lattice of the nanoparticles is perhaps the least explored front. For instance, the energy transfer between a lanthanide donor and an acceptor is generally realized in the form of a dipole–dipole interaction, which is an essential component of the Föster resonance energy transfer (FRET) process. However, cross-interrogation using theoretical and experimental tools suggests that quadruple-quadruple interaction dominates the process of energy transfer, while the exchange mechanism prevails when the donor and acceptor are placed in close proximity.[118] A recently published review article also notes misconceptions and incorrect treatments in estimating the rate of energy transfer.[119] More importantly, the presence of defects significantly complicates the characterization of the energy transfer process. Given the high sensitivity of the acoustic response of defects, the picosecond acoustics-associated method might be useful for probing the spatial distribution of defects and for monitoring the dynamic processes of defect diffusion at the nanoscale.[120]

As a complementary tool to theoretical and experimental approaches, computational simulations provide an additional means to probe the physical and chemical properties of materials at different temporal and spatial scales. Two representative methods are density functional theory and molecular dynamics, which can provide detailed electronic and statistical information. Density functional theory has found various applications in many disciplines by providing accurate ground state electronic structures, which allow us to retrieve the properties of a given material, such as the band gap, orbital alignment, magnetic momentum, and conductivity. Furthermore, high-throughput screening for specific materials can be realized by effectively linking the identity of a material with its specific behavior.[121] Molecular dynamic simulation has been widely employed to study the dynamic and thermodynamic behaviors of nanoparticles.[122,123] These simulations provide a platform with high temporal and spatial precision to retrieve information at the atomic level, which current experimental techniques cannot access. However, the highly localized nature of the f orbitals greatly limits the use of such simulation tools

to probe the luminescence properties of lanthanides. Therefore, advances in computational algorithms could potentially help identify key factors that dictate the energy transfer pathways and thus facilitate the development of high-efficiency upconversion nanoparticles.

■ AUTHOR INFORMATION

Corresponding Author
*E-mail: chmlx@nus.edu.sg.

ORCID ⬤

Xiaogang Liu: 0000-0003-2517-5790

Notes
The authors declare no competing financial interest.

■ REFERENCES

(1) Bloembergen, N. Solid State Infrared Quantum Counters. *Phys. Rev. Lett.* **1959**, *2*, 84−85.

(2) Auzel, F. Upconversion and Anti-Stokes Processes with f and d Ions in Solids. *Chem. Rev.* **2004**, *104*, 139−173.

(3) Ovsyakin, V. V.; Feoflov, P. P. Cooperative Sensitization of Luminescence in Crystals Activated with Rare Earth Ions. *JETP Lett.* **1966**, *4*, 317−318.

(4) Scheps, R. Upconversion Laser Processes. *Prog. Quantum Electron.* **1996**, *20*, 271−358.

(5) Gamelin, D. R.; Gudel, H. U. Upconversion Processes in Transition Metal and Rare Earth Metal Systems. *Top. Curr. Chem.* **2001**, *214*, 1−56.

(6) Johnson, N. J. J.; Oakden, W.; Stanisz, G. J.; Scott Prosser, R.; van Veggel, F. C. J. M. Size-Tunable, Ultrasmall NaGdF₄ Nanoparticles: Insights into Their T₁ MRI Contrast Enhancement. *Chem. Mater.* **2011**, *23*, 3714−3722.

(7) Wang, F.; Liu, X. Upconversion Multicolor Fine-Tuning: Visible to Near-Infrared Emission from Lanthanide-Doped NaYF₄ Nanoparticles. *J. Am. Chem. Soc.* **2008**, *130*, 5642−5643.

(8) Deng, R.; Qin, F.; Chen, R.; Huang, W.; Hong, M.; Liu, X. Temporal Full-Colour Tuning through Non-Steady-State Upconversion. *Nat. Nanotechnol.* **2015**, *10*, 237−242.

(9) Wang, F.; Deng, R.; Wang, J.; Wang, Q.; Han, Y.; Zhu, H.; Chen, X.; Liu, X. Tuning Upconversion through Energy Migration in Core-Shell Nanoparticles. *Nat. Mater.* **2011**, *10*, 968−973.

(10) Han, S.; Deng, R.; Xie, X.; Liu, X. Enhancing Luminescence in Lanthanide-Doped Upconversion Nanoparticles. *Angew. Chem., Int. Ed.* **2014**, *53*, 11702−11715.

(11) Wu, S.; Xia, H.; Xu, J.; Sun, X.; Liu, X. Manipulating Luminescence of Light Emitters by Photonic Crystals. *Adv. Mater.* **2018**, *30*, 1803362.

(12) Wang, F.; Liu, X. Recent Advances in the Chemistry of Lanthanide-Doped Upconversion Nanocrystals. *Chem. Soc. Rev.* **2009**, *38*, 976−989.

(13) Dong, H.; Sun, L. D.; Yan, C. H. Energy Transfer in Lanthanide Upconversion Studies for Extended Optical Applications. *Chem. Soc. Rev.* **2015**, *44*, 1608−1634.

(14) Chen, G.; Qiu, H.; Prasad, P. N.; Chen, X. Upconversion Nanoparticles: Design, Nanochemistry, and Applications in Theranostics. *Chem. Rev.* **2014**, *114*, 5161−5214.

(15) Chan, E. M. Combinatorial Approaches for Developing Upconverting Nanomaterials: High-Throughput Screening, Modeling, and Applications. *Chem. Soc. Rev.* **2015**, *44*, 1653−1679.

(16) Boyer, J. C.; van Veggel, F. C. J. M. Absolute Quantum Yield Measurements of Colloidal NaYF₄: Er³⁺, Yb³⁺ Upconverting Nanoparticles. *Nanoscale* **2010**, *2*, 1417−1419.

(17) Bian, W.; Lin, Y.; Wang, T.; Yu, X.; Qiu, J.; Zhou, M.; Luo, H.; Yu, S. F.; Xu, X. Direct Identification of Surface Defects and Their Influence on the Optical Characteristics of Upconversion Nanoparticles. *ACS Nano* **2018**, *12*, 3623−3628.

(18) Dong, C.; Pichaandi, J.; Regier, T.; van Veggel, F. C. J. M. Nonstatistical Dopant Distribution of Ln³⁺-Doped NaGdF₄ Nanoparticles. *J. Phys. Chem. C* **2011**, *115*, 15950−15958.

(19) Cojocaru, B.; Avram, D.; Kessler, V.; Parvulescu, V.; Seisenbaeva, G.; Tiseanu, C. Nanoscale Insights into Doping Behavior, Particle Size and Surface Effects in Trivalent Metal Doped SnO₂. *Sci. Rep.* **2017**, *7*, 9598.

(20) Rotman, S. R. The Effect of Defects on Inorganic Luminescent Materials. In *Wide-Gap Luminescent Materials: Theory and Applications*; Rotman, S. R., Ed.; Springer US, 1997; Vol. 2, pp 139−190.

(21) Zhou, J.; Wen, S.; Liao, J.; Clarke, C.; Tawfik, S. A.; Ren, W.; Mi, C.; Wang, F.; Jin, D. Activation of the Surface Dark-Layer to Enhance Upconversion in a Thermal Field. *Nat. Photonics* **2018**, *12*, 154−158.

(22) Zou, W.; Visser, C.; Maduro, J. A.; Pshenichnikov, M. S.; Hummelen, J. C. Broadband Dye-Sensitized Upconversion of Near-Infrared Light. *Nat. Photonics* **2012**, *6*, 560−564.

(23) Deng, R.; Wang, J.; Chen, R.; Huang, W.; Liu, X. Enabling Förster Resonance Energy Transfer from Large Nanocrystals through Energy Migration. *J. Am. Chem. Soc.* **2016**, *138*, 15972−15979.

(24) Garfield, D. J.; Borys, N. J.; Hamed, S. M.; Torquato, N. A.; Tajon, C. A.; Tian, B.; Shevitski, B.; Barnard, E. S.; Suh, Y. D.; Aloni, S.; Neaton, J. B.; Chan, E. M.; Cohen, B. E.; Schuck, P. J. Enrichment of Molecular Antenna Triplets Amplifies Upconverting Nanoparticle Emission. *Nat. Photonics* **2018**, *12*, 402−407.

(25) Bao, L.; You, H.; Wang, L.; Li, L.; Qiao, R.; Zhang, Y.; Zhong, Y.; Xiong, Y.; Li, Z. Self-Assembly of LaF₃:Yb,Er/Tm Nanoplates into Colloidal Spheres and Tailoring Their Upconversion Emissions with Fluorescent Dyes. *J. Mater. Chem. C* **2014**, *2*, 8949−8955.

(26) Li, P.; Peng, Q.; Li, Y. Dual-Mode Luminescent Colloidal Spheres from Monodisperse Rare-Earth Fluoride Nanocrystals. *Adv. Mater.* **2009**, *21*, 1945−1948.

(27) Zhao, J.; Wu, J.; Xue, J.; Zhu, Q.; Ni, W. Au/NaYF₄: Yb,Er Binary Superparticles: Synthesis and Optical Properties. *Isr. J. Chem.* **2016**, *56*, 242−248.

(28) Han, S.; Samanta, A.; Xie, X.; Huang, L.; Peng, J.; Park, S. J.; Teh, D. B. L.; Choi, Y.; Chang, Y. T.; All, A. H.; Yang, Y.; Xing, B.; Liu, X. Gold and Hairpin DNA Functionalization of Upconversion Nanocrystals for Imaging and In Vivo Drug Delivery. *Adv. Mater.* **2017**, *29*, 1700244.

(29) Qin, W. P.; Liu, Z. Y.; Sin, C. N.; Wu, C. F.; Qin, G. S.; Chen, Z.; Zheng, K. Z. Multi-ion Cooperative Processes in Yb³⁺ Clusters. *Light: Sci. Appl.* **2014**, *3*, e193.

(30) Wang, J.; Deng, R.; MacDonald, M. A.; Chen, B.; Yuan, J.; Wang, F.; Chi, D.; Hor, T. S. A.; Zhang, P.; Liu, G.; Han, Y.; Liu, X. Enhancing Multiphoton Upconversion through Energy Clustering at Sublattice Level. *Nat. Mater.* **2014**, *13*, 157−162.

(31) Wu, M.; Song, E. H.; Chen, Z. T.; Ding, S.; Ye, S.; Zhou, J. J.; Xu, S. Q.; Zhang, Q. Y. Single-Band Red Upconversion Luminescence of Yb³⁺-Er³⁺ via Nonequivalent Substitution in Perovskite KMgF₃ Nanocrystals. *J. Mater. Chem. C* **2016**, *4*, 1675−1684.

(32) Hu, Y.; Liang, X.; Wang, Y.; Liu, E.; Hu, X.; Fan, J. Enhancement of the Red Upconversion Luminescence in NaYF₄:Yb³⁺, Er³⁺ Nanoparticles by the Transition Metal Ions Doping. *Ceram. Int.* **2015**, *41*, 14545−14553.

(33) Zhu, Y.; Zhao, S.; Zhou, B.; Zhu, H.; Wang, Y. Enhancing Upconversion Luminescence of LiYF₄:Yb,Er Nanocrystals by Cd²⁺ Doping and Core-Shell Structure. *J. Phys. Chem. C* **2017**, *121*, 18909−18916.

(34) Johnson, N. J. J.; He, S.; Diao, S.; Chan, E. M.; Dai, H.; Almutairi, A. Direct Evidence for Coupled Surface and Concentration Quenching Dynamics in Lanthanide-Doped Nanocrystals. *J. Am. Chem. Soc.* **2017**, *139*, 3275−3282.

(35) Rabouw, F. T.; Prins, P. T.; Villanueva-Delgado, P.; Castelijns, M.; Geitenbeek, R. G.; Meijerink, A. Quenching Pathways in NaYF$_4$:Er^{3+},Yb^{3+} Upconversion Nanocrystals. *ACS Nano* **2018**, *12*, 4812−4823.

(36) Hung, P.; Zheng, W.; Zhou, S.; Tu, D.; Chen, Z.; Zhu, H.; Li, R.; Ma, E.; Huang, M.; Chen, X. Lanthanide-Doped LiLuF$_4$ Upconversion Nanoprobes for the Detection of Disease Biomarkers. *Angew. Chem., Int. Ed.* **2014**, *53*, 1252−1257.

(37) Zhuo, Z.; Liu, Y.; Liu, D.; Huang, P.; Jiang, F.; Chen, X.; Hong, M. Manipulating Energy Transfer in Lanthanide-Doped Single Nanoparticles for Highly Enhanced Upconverting Luminescence. *Chem. Sci.* **2017**, *8*, 5050−5056.

(38) Chen, X.; Peng, D.; Ju, Q.; Wang, F. Photon Upconversion in Core–Shell Nanoparticles. *Chem. Soc. Rev.* **2015**, *44*, 1318−1330.

(39) Wu, D. M.; Garcia-Etxarri, A.; Salleo, A.; Dionne, J. A. Plasmon-Enhanced Upconversion. *J. Phys. Chem. Lett.* **2014**, *5*, 4020−4030.

(40) Park, W.; Lu, D.; Ahn, S. Plasmon Enhancement of Luminescence Upconversion. *Chem. Soc. Rev.* **2015**, *44*, 2940−2962.

(41) Xu, W.; Chen, X.; Song, H. Upconversion Manipulation by Local Electromagnetic Field. *Nano Today* **2017**, *17*, 54−78.

(42) Saboktakin, M.; Ye, X.; Chettiar, U. K.; Engheta, N.; Murray, C. B.; Kagan, C. R. Plasmonic Enhancement of Nanophosphor Upconversion Luminescence in Au Nanohole Arrays. *ACS Nano* **2013**, *7*, 7186−7192.

(43) Greybush, N. J.; Saboktakin, M.; Ye, X.; Giovampaola, C. D.; Oh, S. J.; Berry, N. E.; Engheta, N.; Murray, C. B.; Kagan, C. R. Plasmon-Enhanced Upconversion Luminescence in Single Nano-phosphor-Nanorod Heterodimers Formed through Template-Assisted Self-Assembly. *ACS Nano* **2014**, *8*, 9482−9491.

(44) Yin, Z.; Li, H.; Xu, W.; Cui, S.; Zhou, D.; Chen, X.; Zhu, Y.; Qin, G.; Song, H. Local Field Modulation Induced Three-Order Upconversion Enhancement: Combining Surface Plasmon Effect and Photonic Crystal Effect. *Adv. Mater.* **2016**, *28*, 2518−2525.

(45) Bang, D.; Jo, E. J.; Hong, S.; Byun, J. Y.; Lee, J. Y.; Kim, M. G.; Lee, L. P. Asymmetric Nanocrescent Antenna on Upconversion Nanocrystal. *Nano Lett.* **2017**, *17*, 6583−6590.

(46) Sun, Q. C.; Mundoor, H.; Ribot, J. C.; Singh, V.; Smalyukh, I. I.; Nagpal, P. Plasmon-Enhanced Energy Transfer for Improved Upconversion of Infrared Radiation in Doped-Lanthanide Nanocryst-als. *Nano Lett.* **2014**, *14*, 101−106.

(47) Lu, D.; Cho, S. K.; Ahn, S.; Brun, L.; Summers, C. J.; Park, W. Plasmon Enhancement Mechanism for the Upconversion Processes in NaYF$_4$:Yb^{3+},Er^{3+} Nanoparticles: Maxell versus Föster. *ACS Nano* **2014**, *8*, 7780−7792.

(48) Lu, D.; Mao, C.; Cho, S. K.; Ahn, S.; Park, W. Experimental Demonstration of Plasmon Enhanced Energy Transfer Rate in NaYF$_4$:Yb^{3+},Er^{3+} Upconversion Nanoparticles. *Sci. Rep.* **2016**, *6*, 18894.

(49) Wang, Y.; Yang, Z.; Ma, Y.; Chai, Z.; Qiu, J.; Song, Z. Upconversion Emission Enhancement Mechanism of Nd^{3+}−Sensi-tized NaYF$_4$:Yb^{3+},Er^{3+} Nanoparticles using Tunable Plasmonic Au Films: Plasmonic-Induced Excitation, Radiative Decay Rate and Energy-Transfer Enhancement. *J. Mater. Chem. C* **2017**, *5*, 8535−8544.

(50) Das, A.; Mao, C.; Cho, S.; Kim, K.; Park, W. Over 1000-Fold Enhancement of Upconversion Luminescence using Water-Disper-sible Metal-Insulator-Metal Nanostructures. *Nat. Commun.* **2018**, *9*, 4828.

(51) Drees, C.; Raj, A. N.; Kurre, R.; Busch, K. B.; Haase, M.; Piehler, J. Engineered Upconversion Nanoparticles for Resolving Protein Interactions inside Living Cells. *Angew. Chem., Int. Ed.* **2016**, *55*, 11668−11672.

(52) Zheng, W.; Huang, P.; Tu, D.; Ma, E.; Zhu, H.; Chen, X. Lanthanide-Doped Upconversion Nano-Bioprobes: Electronic Struc-

(53) Yang, Y.; Shao, Q.; Deng, R.; Wang, C.; Teng, X.; Cheng, K.; Cheng, Z.; Huang, L.; Liu, Z.; Liu, X.; Xing, B. In Vitro and In Vivo Uncaging and Bioluminescence Imaging by using Photocaged Upconversion Nanoparticles. *Angew. Chem., Int. Ed.* **2012**, *51*, 3125−3129.

(54) Zhou, J.; Liu, Q.; Feng, W.; Sun, Y.; Li, F. Upconversion Luminescent Materials: Advances and Applications. *Chem. Rev.* **2015**, *115*, 395−465.

(55) Brites, C. D. S.; Xie, X.; Debasu, M. L.; Qin, X.; Chen, R.; Huang, W.; Rocha, J.; Liu, X.; Carlos, L. D. Instantaneous Ballistic Velocity of Suspended Brownian Nanocrystals Measured by Upconversion Nanothermometry. *Nat. Nanotechnol.* **2016**, *11*, 851−856.

(56) Abbe, E. Beiträge zur Theorie des Mikroskops und der mikroskopischen Wahrnehmung. *Arch. für Mikroskopische Anat.* **1873**, *9*, 413−418.

(57) Neupane, B.; Ligler, F. S.; Wang, G. Review of Recent Developments in Stimulated Emission Depletion Microscopy: Applications on Cell Imaging. *J. Biomed. Opt.* **2014**, *19*, 080901.

(58) Hiersemenzel, K.; Brown, E. R.; Duncan, R. R. Imaging Large Cohorts of Single Ion Channels and Their Activity. *Front. Endocrinol.* **2013**, *4*, 114.

(59) Wang, Y. F.; Liu, G. Y.; Sun, L. D.; Xiao, J. W.; Zhou, J. C.; Yan, C. H. Nd^{3+}-sensitized Upconversion Nanophosphors: Efficient In Vivo Bioimaging Probes with Minimized Heating Effect. *ACS Nano* **2013**, *7*, 7200−7206.

(60) Xie, X.; Gao, N.; Deng, R.; Sun, Q.; Xu, Q. H.; Liu, X. Mechanistic Investigation of Photon Upconversion in Nd^{3+}-Sensitized Core−Shell Nanoparticles. *J. Am. Chem. Soc.* **2013**, *135*, 12608−12611.

(61) Zhong, Y.; Tian, G.; Gu, Z.; Yang, Y.; Gu, L.; Zhao, Y.; Ma, Y.; Yao, J. Elimination of Photon Quenching by a Transition Layer to Fabricate a Quenching-Shield Sandwich Structure for 800 nm Excited Upconversion Luminescence of Nd^{3+}-Sensitized Nanoparticles. *Adv. Mater.* **2014**, *26*, 2831−2837.

(62) Dong, H.; Du, S. R.; Zheng, X. Y.; Lyu, G. M.; Sun, L. D.; Li, L. D.; Zhang, P. Z.; Zhang, C.; Yan, C. H. Lanthanide Nanoparticles: From Design toward Bioimaging and Therapy. *Chem. Rev.* **2015**, *115*, 10725−10815.

(63) Fan, Y.; Wang, P.; Lu, Y.; Wang, R.; Zhou, L.; Zheng, X.; Li, X.; Piper, J. A.; Zhang, F. Lifetime-Engineered NIR-II Nanoparticles Unlock Multiplexed In Vivo Imaging. *Nat. Nanotechnol.* **2018**, *13*, 941−946.

(64) Kolesov, R.; Reuter, R.; Xia, K.; Stöhr, R.; Zappe, A.; Wrachtrup, J. Super-Resolution Upconversion Microscopy of Praseodymium-Doped Yttrium Aluminum Garnet Nanoparticles. *Phys. Rev. B: Condens. Matter Mater. Phys.* **2011**, *84*, 153413.

(65) Wu, R.; Zhan, Q.; Liu, H.; Wen, X.; Wang, B.; He, S. Optical Depletion Mechanism of Upconverting Luminescence and Its Potential for Multi-Photon STED-Like Microscopy. *Opt. Express* **2015**, *23*, 32401.

(66) Liu, Y.; Lu, Y.; Yang, X.; Zheng, X.; Wen, S.; Wang, F.; Vidal, X.; Zhao, J.; Liu, D.; Zhou, Z.; Ma, C.; Zhou, J.; Piper, J. A.; Xi, P.; Jin, D. Amplified Stimulated Emission in Upconversion Nanoparticles for Super-Resolution Nanoscopy. *Nature* **2017**, *543*, 229−233.

(67) Zhan, Q.; Liu, H.; Wang, B.; Wu, Q.; Pu, R.; Zhou, C.; Huang, B.; Peng, X.; Agren, H.; He, S. Achieving High-Efficiency Emission Depletion Nanoscopy by Employing Cross Relaxation in Upconver-sion Nanoparticles. *Nat. Commun.* **2017**, *8*, 1058.

(68) Zhang, H.; Jia, T.; Chen, L.; Zhang, Y.; Zhang, S.; Feng, D.; Sun, Z.; Qiu, J. Depleted Upconversion Luminescence in NaYF$_4$:Yb^{3+},Tm^{3+} Nanoparticles via Simultaneous Two-Wavelength Excitation. *Phys. Chem. Chem. Phys.* **2017**, *19*, 17756−17764.

(69) Shin, K.; Jung, T.; Lee, E.; Lee, G.; Goh, Y.; Heo, J.; Jung, M.; Jo, E. J.; Lee, H.; Kim, M. G.; Lee, K. T. Distinct Mechanisms for the Upconversion of NaYF$_4$:Yb^{3+},Er^{3+} Nanoparticles Revealed by

Stimulated Emission Depletion. *Phys. Chem. Chem. Phys.* **2017**, *19*, 9739−9744.

(70) Deisseroth, K.; Anikeeva, P. Upconversion of Light for Use in Optogenetic Methods. *United States Patent*, PCT/US11/59287, 2011.

(71) Shah, S.; Liu, J. J.; Pasquale, N.; Lai, J.; McGowan, H.; Pang, Z. P.; Lee, K. B. Hybrid Upconversion Nanomaterials for Optogenetic Neuronal Control. *Nanoscale* **2015**, *7*, 16571−16577.

(72) Hososhima, S.; Yuasa, H.; Ishizuka, T.; Hoque, M. R.; Yamashita, T.; Yamanaka, A.; Sugano, E.; Tomita, T.; Yawo, H. Near-Infrared (NIR) Up-Conversion Optogenetics. *Sci. Rep.* **2015**, *5*, 16533.

(73) He, L.; Zhang, Y.; Ma, G.; Tan, P.; Li, Z.; Zang, S.; Wu, X.; Jing, J.; Fang, S.; Zhou, L.; Wang, Y.; Huang, Y.; Hogan, P. G.; Han, G.; Zhou, Y. Near-Infrared Photoactivatable Control of Ca^{2+} Signaling and Optogenetic Immunomodulation. *eLife* **2015**, *4*, e10024.

(74) Bansal, A.; Liu, H.; Jayakumar, M. K. G.; Andersson-Engels, S.; Zhang, Y. Quasi-Continuous Wave Near-Infrared Excitation of Upconversion Nanoparticles for Optogenetic Manipulation of C. elegans. *Small* **2016**, *12*, 1732−1743.

(75) Ai, X.; Lyu, L.; Zhang, Y.; Tang, Y.; Mu, J.; Liu, F.; Zhou, Y.; Zuo, Z.; Liu, G.; Xing, B. Remote Regulation of Membrane Channel Activity by Site-Specific Localization of Lanthanide-Doped Upconversion Nanocrystals. *Angew. Chem., Int. Ed.* **2017**, *56*, 3031−3035.

(76) Pliss, A.; Ohulchanskyy, T. Y.; Chen, G.; Damasco, J.; Bass, C. E.; Prasad, P. N. Subcellular Optogenetics Enacted by Targeted Nanotransformers of Near-Infrared Light. *ACS Photonics* **2017**, *4*, 806−814.

(77) Lin, X.; Wang, Y.; Chen, X.; Yang, R.; Wang, Z.; Feng, J.; Wang, H.; Lai, K. W. C.; He, J.; Wang, F.; Shi, P. Multiplexed Optogenetic Stimulation of Neurons with Spectrum-Selective Upconversion Nanoparticles. *Adv. Healthcare Mater.* **2017**, *6*, 1700446.

(78) Wang, Y.; Lin, X.; Chen, X.; Chen, X.; Xu, Z.; Zhang, W.; Liao, Q.; Duan, X.; Wang, X.; Liu, M.; Wang, F.; He, J.; Shi, P. Tetherless Near-Infrared Control of Brain Activity in Behaving Animals using Fully Implantable Upconversion Microdevices. *Biomaterials* **2017**, *142*, 136−148.

(79) Lin, X.; Chen, X.; Zhang, W.; Sun, T.; Fang, P.; Liao, Q.; Chen, X.; He, J.; Liu, M.; Wang, F.; Shi, P. Core-Shell-Shell Upconversion Nanoparticles with Enhanced Emission for Wireless Optogenetic Inhibition. *Nano Lett.* **2018**, *18*, 948−956.

(80) Chen, S.; Weitemier, A. Z.; Zeng, X.; He, L.; Wang, X.; Tao, Y.; Huang, A. J. Y.; Hashimotodani, Y.; Kano, M.; Iwasaki, H.; Parajuli, L. K.; Okabe, S.; Teh, D. B. L.; All, A. H.; Tsutsui-Kimura, I.; Tanaka, K. F.; Liu, X.; McHugh, T. J. Near-Infrared Stimulation via Upconversion Nanoparticle−Mediated Optogenetics. *Science* **2018**, *359*, 679−684.

(81) Zheng, B.; Wang, H.; Pan, H.; Liang, C.; Ji, W.; Zhao, L.; Chen, H.; Gong, X.; Wu, X.; Chang, J. Near-Infrared Light Triggered Upconversion Optogenetic Nanosystem for Cancer Therapy. *ACS Nano* **2017**, *11*, 11898−11907.

(82) Zhao, J.; Jin, D.; Schartner, E. P.; Lu, Y.; Liu, Y.; Zvyagin, A. V.; Zhang, L.; Dawes, J. M.; Xi, P.; Piper, J. A.; Goldys, E. M.; Monro, T. M. Single-Nanocrystal Sensitivity Achieved by Enhanced Upconversion Luminescence. *Nat. Nanotechnol.* **2013**, *8*, 729−734.

(83) Gargas, D. J.; Chan, E. M.; Ostrowski, A. D.; Aloni, S.; Altoe, M. V. P.; Barnard, E. S.; Sanii, B.; Urban, J. J.; Milliron, D. J.; Cohen, B. E.; Schuck, P. J. Engineering Bright Sub-10-nm Upconverting Nanocrystals for Single-Molecule Imaging. *Nat. Nanotechnol.* **2014**, *9*, 300−305.

(84) Liu, Q.; Zhang, Y.; Peng, C. S.; Yang, T.; Joubert, L. M.; Chu, S. Single Upconversion Nanoparticle Imaging at Sub-10 W cm^{-2} Irradiance. *Nat. Photonics* **2018**, *12*, 548−553.

(85) Wu, X.; Zhang, Y.; Takle, K.; Bilsel, O.; Li, Z.; Lee, H.; Zhang, Z.; Li, D.; Fan, W.; Duan, C.; Chan, E. M.; Lois, C.; Xiang, Y.; Han, G. Dye-Sensitized Core/Active Shell Upconversion Nanoparticles for Optogenetics and Bioimaging Applications. *ACS Nano* **2016**, *10*, 1060−1066.

(86) Feliu, N.; Neher, E.; Parak, W. J. Toward an Optically Controlled Brain. *Science* **2018**, *359*, 633−634.

(87) Johnson, L. F.; Guggenheim, H. J. Infrared-Pumped Visible Laser. *Appl. Phys. Lett.* **1971**, *19*, 44−47.

(88) Zhu, H.; Chen, X.; Jin, L. M.; Wang, Q. J.; Wang, F.; Yu, S. F. Amplified Spontaneous Emission and Lasing from Lanthanide-Doped Up-Conversion Nanocrystals. *ACS Nano* **2013**, *7*, 11420−11426.

(89) Chen, X.; Jin, L.; Kong, W.; Sun, T.; Zhang, W.; Liu, X.; Fan, J.; Yu, S. F.; Wang, F. Confining Energy Migration in Upconversion Nanoparticles towards Deep Ultraviolet Lasing. *Nat. Commun.* **2016**, *7*, 10304.

(90) Wang, T.; Yu, H.; Siu, C. K.; Qiu, J.; Xu, X.; Yu, S. F. White-Light Whispering-Gallery-Mode Lasing from Lanthanide-Doped Upconversion $NaYF_4$ Hexagonal Microrods. *ACS Photonics* **2017**, *4*, 1539−1543.

(91) Fernandez-Bravo, A.; Yao, K.; Barnard, E. S.; Borys, N. J.; Levy, E. S.; Tian, B.; Tajon, C. A.; Moretti, L.; Altoe, M. V.; Aloni, S.; Beketayev, K.; Scotognella, F.; Cohen, B. E.; Chan, E. M.; Schuck, P. J. Continuous-Wave Upconverting Nanoparticle Microlasers. *Nat. Nanotechnol.* **2018**, *13*, 572−577.

(92) Yao, W.; Tian, Q.; Liu, J.; Wu, Z.; Cui, S.; Ding, J.; Dai, Z.; Wu, W. Large-Scale Synthesis and Screen Printing of Upconversion Hexagonal-Phase $NaYF_4:Yb^{3+},Tm^{3+}/Er^{3+}/Eu^{3+}$ Plates for Security Applications. *J. Mater. Chem. C* **2016**, *4*, 6327−6335.

(93) Meruga, J. M.; Baride, A.; Cross, W.; Kellar, J. J.; May, P. S. Red-Green-Blue Printing using Luminescence-Upconversion Inks. *J. Mater. Chem. C* **2014**, *2*, 2221−2227.

(94) Zhang, Y.; Zhang, L.; Deng, R.; Tian, J.; Zong, Y.; Jin, D.; Liu, X. Multicolor Barcoding in a Single Upconversion Crystal. *J. Am. Chem. Soc.* **2014**, *136*, 4893−4896.

(95) Lee, J.; Bisso, P. W.; Srinivas, R. L.; Kim, J. J.; Swiston, A. J.; Doyle, P. S. Universal Process-Inert Encoding Architecture for Polymer Microparticles. *Nat. Mater.* **2014**, *13*, 524−529.

(96) You, M.; Zhong, J.; Hong, Y.; Duan, Z.; Lin, M.; Xu, F. Inkjet Printing of Upconversion Nanoparticles for Anti-Counterfeit Applications. *Nanoscale* **2015**, *7*, 4423−4431.

(97) Li, M.; Yao, W.; Liu, J.; Tian, Q.; Liu, L.; Ding, J.; Xue, Q.; Lu, Q.; Wu, W. Facile Synthesis and Screen Printing of Dual-Mode Luminescent $NaYF_4$:Er,Yb (Tm)/Carbon Dots for Anti-Counterfeiting Applications. *J. Mater. Chem. C* **2017**, *5*, 6512−6520.

(98) Zheng, W.; Huang, P.; Gong, Z.; Tu, D.; Xu, J.; Zou, Q.; Li, R.; You, W.; Bünzli, J. C. G.; Chen, X. Near-Infrared-Triggered Photon Upconversion Tuning in All-Inorganic Cesium Lead Halide Perovskite Quantum Dots. *Nat. Commun.* **2018**, *9*, 3462.

(99) Sun, T.; Xu, B.; Chen, B.; Chen, X.; Li, M.; Shi, P.; Wang, F. Anti-Counterfeiting Patterns Encrypted with Multi-Mode Luminescent Nanotaggants. *Nanoscale* **2017**, *9*, 2701−2705.

(100) Liu, Y.; Tu, D.; Zhu, H.; Li, R.; Luo, W.; Chen, X. A Strategy to Achieve Efficient Dual-Mode Luminescence of Eu^{3+} in Lanthanides Doped Multifunctional $NaGdF_4$ nanocrystals. *Adv. Mater.* **2010**, *22*, 3266−3271.

(101) Kumar, P.; Dwivedi, J.; Gupta, B. K. Highly Luminescent Dual Model Rare-Earth Nanorod Assisted Multi-Stage Excitable Security Ink for Anti-Counterfeiting Applications. *J. Mater. Chem. C* **2014**, *2*, 10468−10475.

(102) Han, Y.; Li, H.; Wang, Y.; Pan, Y.; Huang, L.; Song, F.; Huang, W. Upconversion Modulation through Pulsed Laser Excitation for Anti-counterfeiting. *Sci. Rep.* **2017**, *7*, 1320.

(103) Zhou, D.; Li, D.; Zhou, X.; Xu, W.; Chen, X.; Liu, D.; Zhu, Y.; Song, H. Semiconductor Plasmon Induced Upconversion Enhancement in $mCu_{2-x}S@SiO_2@Y_2O_3:Yb^{3+},Er^{3+}$ Core-Shell Nanocomposites. *ACS Appl. Mater. Interfaces* **2017**, *9*, 35226−35233.

(104) Liu, H.; Jayakumar, M. K. G.; Huang, K.; Wang, Z.; Zheng, X.; Agren, H.; Zhang, Y. Phase Angle Encoded Upconversion Luminescent Nanocrystals for Multiplexing Applications. *Nanoscale* **2017**, *9*, 1676−1686.

(105) Lu, Y.; Zhao, J.; Zhang, R.; Liu, Y.; Liu, D.; Goldys, E. M.; Yang, X.; Xi, P.; Sunna, A.; Lu, J.; Shi, Y.; Leif, R. C.; Huo, Y.; Shen, J.; Piper, J. A.; Robinson, J. P.; Jin, D. Tunable Lifetime Multiplexing using Luminescent Nanocrystals. *Nat. Photonics* **2014**, *8*, 32−36.

(106) Dong, H.; Sun, L. D.; Feng, W.; Gu, Y.; Li, F.; Yan, C. H. Versatile Spectral and Lifetime Multiplexing Nanoplatform with Excitation Orthogonalized Upconversion Luminescence. *ACS Nano* **2017**, *11*, 3289−3297.

(107) Liu, X.; Wang, Y.; Li, X.; Yi, Z.; Deng, R.; Liang, L.; Xie, X.; Loong, D. T. B.; Song, S.; Fan, D.; All, A. H.; Zhang, H.; Huang, L.; Liu, X. Binary Temporal Upconversion Codes of Mn^{2+}-Activated Nanoparticles for Multilevel Anti-Counterfeiting. *Nat. Commun.* **2017**, *8*, 899.

(108) Lei, L.; Chen, D.; Li, C.; Huang, F.; Zhang, J.; Xu, S. Inverse Thermal Quenching Effect in Lanthanide-Doped Upconversion Nanocrystals for Anti-Counterfeiting. *J. Mater. Chem. C* **2018**, *6*, 5427−5433.

(109) Wu, Q.; Huang, B.; Peng, X.; He, S.; Zhan, Q. Non-Bleaching Fluorescence Emission Difference Microscopy using Single 808-nm Laser Excited Red Upconversion Emission. *Opt. Express* **2017**, *25*, 30885.

(110) Chen, C.; Wang, F.; Wen, S.; Su, Q. P.; Wu, M. C. L.; Liu, Y.; Wang, B.; Li, D.; Shan, X.; Kianinia, M.; Aharonovich, I.; Toth, M.; Jackson, S. P.; Xi, P.; Jin, D. Multi-Photon Near-Infrared Emission Saturation Nanoscopy using Upconversion Nanoparticles. *Nat. Commun.* **2018**, *9*, 3290.

(111) Huang, X.; Han, S.; Huang, W.; Liu, X. Enhancing Solar Cell Efficiency: the Search for Luminescent Materials as Spectral Converters. *Chem. Soc. Rev.* **2013**, *42*, 173−201.

(112) Van Sark, W. G.; de Wild, J.; Rath, J. K.; Meijerink, A.; Schropp, R. E. Upconversion in Solar Cells. *Nanoscale Res. Lett.* **2013**, *8*, 81.

(113) Goldschmidt, J. C.; Fischer, S. Upconversion for Photovoltaics − A Review of Materials, Devices and Concepts for Performance Enhancement. *Adv. Opt. Mater.* **2015**, *3*, 510−535.

(114) He, M.; Pang, X.; Liu, X.; Jiang, B.; He, Y.; Snaith, H.; Lin, Z. Monodisperse Dual-Functional Upconversion Nanoparticles Enabled Near-Infrared Organolead Halide Perovskite Solar Cells. *Angew. Chem., Int. Ed.* **2016**, *55*, 4280−4284.

(115) Roh, J.; Yu, H.; Jang, J. Hexagonal β-$NaYF_4$:Yb^{3+}, Er^{3+} Nanorpism-Incorporated Upconverting Layer in Perovskite Solar Cells for Near-Infrared Sunlight Harvesting. *ACS Appl. Mater. Interfaces* **2016**, *8*, 19847−19852.

(116) Arnaoutakis, G. E.; Marques-Hueso, J.; Ivaturi, A.; Fischer, S.; Goldschmidt, J. C.; Krämer, K. W.; Richards, B. S. Enhanced Energy Conversion of Up-Conversion Solar Cells by the Integration of Compound Parabolic Concentrating Optics. *Sol. Energy Mater. Sol. Cells* **2015**, *140*, 217−223.

(117) Park, J. E.; Jung, Y.; Kim, M.; Nam, J. M. Quantitative Nanoplasmonics. *ACS Cent. Sci.* **2018**, *4*, 1303−1314.

(118) Malta, O. L. Mechanisms of Non-Radiative Energy Transfer Involving Lanthanide Ions Revisited. *J. Non-Cryst. Solids* **2008**, *354*, 4770−4776.

(119) Tanner, P. A.; Zhou, L.; Duan, C.; Wong, K. L. Misconceptions in Electronic Energy Transfer: Bridging the Gap Between Chemistry and Physics. *Chem. Soc. Rev.* **2018**, *47*, 5234−5265.

(120) Zhang, Y.; Kurt, O.; Ascienzo, D.; Yang, Q.; Le, T.; Greenbaum, S.; Bayer, T. J. M.; Randall, C. A.; Ren, Y. Detection of Nanoscale Structural Defects in Degraded Fe-Doped $SrTiO_3$ by Ultrafast Photoacoustic Waves. *J. Phys. Chem. C* **2018**, *122*, 12864−12868.

(121) Qin, X.; Liu, X.; Huang, W.; Bettinelli, M.; Liu, X. Lanthanide-Activated Phosphors Based on 4f-5d Optical Transitions: Theoretical and Experimental Aspects. *Chem. Rev.* **2017**, *117*, 4488−4527.

(122) Luo, M.; Mazyar, O. A.; Zhu, Q.; Vaughn, M. W.; Hase, W. L.; Dai, L. L. Molecular Dynamics Simulation of Nanoparticle Self-Assembly at a Liquid-Liquid Interface. *Langmuir* **2006**, *22*, 6385−6390.

(123) Tian, P. Molecular Dynamics Simulations of Nanoparticles. *Annu. Rep. Prog. Chem., Sect. C: Phys. Chem.* **2008**, *104*, 142−164.